Enhanced Power Conversion Efficiency of Inverted Organic Solar Cells with a Ga-Doped ZnO Nanostructured Thin Film Prepared Using Aqueous Solution

Kyung-Sik Shin,[†] Kang-Hyuck Lee,[†] Hyun Hwi Lee,[‡] Dukhyun Choi,*[,§] and Sang-Woo Kim*[,†,∥]

School of Advanced Materials Science and Engineering, Sungkyunkwan University, Suwon 440-746, Republic of Korea, Pohang Accelerator Laboratory, POSTECH, Pohang, Gyeongbuk 790-784, Republic of Korea, Department of Mechanical Engineering, Kyung Hee University, Yongin, Gyeonggi 449-701, Republic of Korea, and SKKU Advanced Institute of Nanotechnology (SAINT) and Center for Human Interface Nanotechnology (HINT), Sungkyunkwan University, Suwon 440-746, Republic of Korea

Received: February 12, 2010; Revised Manuscript Received: June 8, 2010

A dramatic increase in the power conversion efficiency (PCE) of inverted organic solar cells (IOSCs) is realized by a gallium (Ga)-doped zinc oxide (GZO) buffer layer acting as an electron-transport layer. The GZO nanostructured thin-film buffer layer was synthesized via an aqueous solution method at 90 °C. Both an increase of electrical conductivity and a smooth surface morphology were realized by Ga doping. The PCE of a GZO-based IOSC was improved by about 110% at simulated air mass 1.5 global full-sun illumination compared with that of undoped zinc oxide-based IOSCs. The increase of the short-circuit current in GZO-based IOSCs is due to the higher electron conductivity and favorable surface morphology of the buffer layer through Ga-doping, resulting in the dramatic enhancement of the PCE.

1. Introduction

Solution-processed organic solar cells (OSCs) are of great interest due to their low cost, large size, and easily printable fabrication method.[1−3] However, the short exciton diffusion length and inefficient exciton dissociation in a polymeric matrix result in a low quantum efficiency (QE), limiting the applications of OSCs.[4,5] A major breakthrough was achieved through the bulk heterojunction (BHJ) concept based on a polymer:fullerene structure where the nanoscale phase separation creates donor/acceptor interfaces for effective exciton dissociation via efficient charge transfer from donor to acceptor.[6,7] Despite the high attainable QE, the overall power conversion efficiency (PCE) is still low due to the interior charge-transport properties.

So far, studies regarding the realization of highly efficient BHJ solar cells have focused on the solvent selection, annealing control, and work function engineering.[7,8] Plasma treatment or a self-assembled monolayer, for example, was applied to a buffer layer on which a photoactive polymer is spin-coated in order to control the polymer morphology and optimize the work function.[9] It is well known that the use of a doping approach can improve the electrical conductivity (σ) of semiconducting materials with no significant change of the band gap between p−n materials. Furthermore, it has been studied that doping has a large effect on the surface morphologies of as-grown thin films.[10,11] However, studies have rarely reported on the effect of doping on solar power performance.[12]

Herein, we report a dramatic increase in the PCE of inverted organic solar cells (IOSCs) by a gallium (Ga)-doped zinc oxide (GZO) buffer layer acting as an electron-transport layer. This method involves the growth of GZO nanostructured thin films by a simple aqueous solution route, at the low temperature of 90 °C. This is a simple and effective process for improving the PCE of IOSCs. Compared with undoped zinc oxide (UZO)-based IOSCs, the PCE of the IOSCs with the GZO buffer layer was increased by about 110% at simulated air mass (AM) 1.5 global full-sun (1.5G, 100 mW/cm^2) illumination.

2. Experimental Section

The UZO and GZO thin films were synthesized using a two-step solution process. The first step for both the UZO and the GZO buffer layers is seed layer preparation. The seed layer for UZO was prepared on an indium tin oxide/glass substrate by dip-coating into 0.05 M zinc acetate ($Zn(C_2H_3O_2)_2$) dissolved ethanol solution. For the seed solution of GZO, a mixture of Ga nitrate ($Ga(NO_3)_3 \cdot xH_2O$) and zinc acetate in a mass ratio of 1:9 was dissolved in ethanol, leading to an n-type doping. The second step in the synthesis is the main growth of the each layer. A UZO layer was formed in a solution of 50 mM zinc nitrate hexahydrate ($Zn(NO_3)_2 \cdot 6H_2O$) and 50 mM hexamethylenetetramine ($C_6H_{12}N_4$) dissolved in ethanol/DI water (vol % = 1:1) at 90 °C for 3 h. A GZO buffer layer was synthesized in the solution in which Ga nitrate (10% of zinc nitrate hexahydrate in a mass ratio) was added into the solution for the main growth of a UZO layer. This solution-based fabrication process for a buffer layer provides many promising advantages, such as low cost, low temperature, and damage-free.[13,14]

To produce inverted IOSCs based on UZO and GZO buffer layers, a polymer blend of poly(3-hexylthiophene) (P3HT):(6,6)-phenyl C_{61} butyric acid methyl ester (PCBM) (1:1 vol % in chlorobenzene) was spin-coated onto both buffer layers at 2000 rpm for 120 s and was dried in covered glass Petri dishes (solvent annealing[2,8]). Thermal annealing at 150 °C for 10 min was then carried out. Molybdenum oxide (MoO_3) as an electron-blocking layer and a gold (Au) anode were subsequently deposited by thermal evaporation. Ga doping to ZnO was confirmed using X-ray photoelectron spectroscopy (XPS) and synchrotron X-ray diffraction (XRD) measurements. Morphol-

* To whom correspondence should be addressed. E-mail: kimsw1@skku.edu (S.-W.K.), dchoi@khu.ac.kr (D.C.).
† School of Advanced Materials Science and Engineering, Sungkyunkwan University.
‡ POSTECH.
§ Kyung Hee University.
∥ SAINT and HINT, Sungkyunkwan University.

10.1021/jp1013658

ogies of UZO and GZO thin films prepared using the solution method were examined by atomic force microscopy (AFM) measurements. Contact angles for each sample of UZO and GZO were also measured by water contact angle measurements. For the characterizations of IOSCs, current density−voltage ($J-V$) measurements were carried out by using a solar simulator under an irradiation intensity of air mass AM 1.5G (100 mW/cm^2). We obtained our results from over 50 IOSCs for UZO and GZO, respectively.

3. Results and Discussion

A field emission scanning electron microscopy (FE-SEM) image in Figure 1a shows the typical surface morphology of the grown GZO nanostructured thin film. The GZO thin film comprising dense nanorod arrays with a *c*-axis preferred orientation was grown in aqueous solution. Although the thin film has a vertically textured morphology, it was found that the vertically aligned nanorods are also laterally connected to one another. A cross-sectional FE-SEM image and a schematic illustration of our inverted IOSC structure using the GZO are revealed in Figure 1b,c, respectively. The total thickness of our inverted IOSC was about 850 nm, and the thickness of the GZO layers was about 270 nm. The polymer layer was 180 nm thick. The structural dimensions of the UZO-based IOSCs were the same as those of the GZO-based IOSCs.

The doping of Ga into ZnO was examined using XPS and synchrotron XRD measurements. The XPS survey for the Ga element in the GZO thin film is shown in Figure 2a. The two peaks at 1117.4 and 1144.4 eV are ascribed to the electronic states of Ga $2p_{3/2}$ and Ga $2p_{1/2}$, respectively; that energy gap is consistent with the value for the element, about 27 eV. The Ga $2p_{3/2}$ peaks of the UZO and GZO thin films are shown in Figure 2b. In the GZO thin film, a broad peak assigned to the electronic state of Ga $2p_{3/2}$ is clearly observed, whereas in the UZO thin film, no peak related to the Ga element is detected. The clear appearance of the Ga-related peak in the GZO sample indicates that Ga atoms were doped effectively into the ZnO lattices.[15,16]

Figure 3 shows (002) diffraction peaks of the UZO and GZO thin films in the power diffraction profiles from a synchrotron X-ray source. The scans were taken along the surface normal direction, $Q_z[Q = 4\pi \sin(2\theta/2)/\lambda]$, in reciprocal space. The (002) peak position (2.415 Å^{-1}) of the GZO thin film was slightly shifted to a higher Q_z value compared with that (2.412 Å^{-1}) of the UZO thin film. This shift means that there is tensile stress in the plane of the GZO thin film as compared with the UZO thin film, which may originate from the difference of the radii of Ga^{3+} (0.062 nm) and Zn^{2+} (0.074 nm). The replacement of Zn^{2+} with Ga^{3+} decreases the *c*-axis lattice parameter, resulting in an increase of the diffraction angle.[17,18] In addition, we could not observe any pure Ga or Ga_2O_3-related diffraction peaks in the high-resolution synchrotron XRD measurements.

AFM measurements reveal that root-mean-square (rms) roughness values of UZO and GZO surfaces were 10.7 and 4.6 nm, respectively (Figure 4). The rms roughness and the grain size of the grown thin films are decreased upon addition of Ga (see Figure 4), showing good agreement with the previous reports.[10,11] To understand the surface property of the UZO and GZO thin films, we also measured the contact angles (CAs) via water contact angle measurements. As shown in the insets of Figure 4, the CAs for the UZO and GZO thin films were 87.9° and 69.9°, respectively, demonstrating a higher hydrophilicity on GZO than on UZO.

To compare the solar power performances of IOSCs based on UZO and GZO, current density−voltage ($J-V$) measurements were carried out by using a solar simulator under standard AM 1.5G solar illumination. Figure 5 shows $J-V$ curves for IOSCs with UZO or GZO buffer layers acting as the electron-transport layer under AM 1.5G irradiation. The GZO-based IOSC averagely exhibited an open-circuit voltage (V_{oc}) of 0.42 V, a short-circuit current (J_{sc}) of 11.7 mA/cm^2, a fill factor (FF) of 39.7%, and a PCE of 1.95%, whereas the UZO-based IOSC averagely showed the V_{oc} of 0.41 V, the J_{sc} of 6.3 mA/cm^2, the FF of 35.7%, and the PCE of 0.92%. These data demonstrate that the PCE can be enhanced more than about 2 times by doping Ga into ZnO. The significant enhancement of the PCE in GZO-based IOSCs could be attributed to the improved σ of

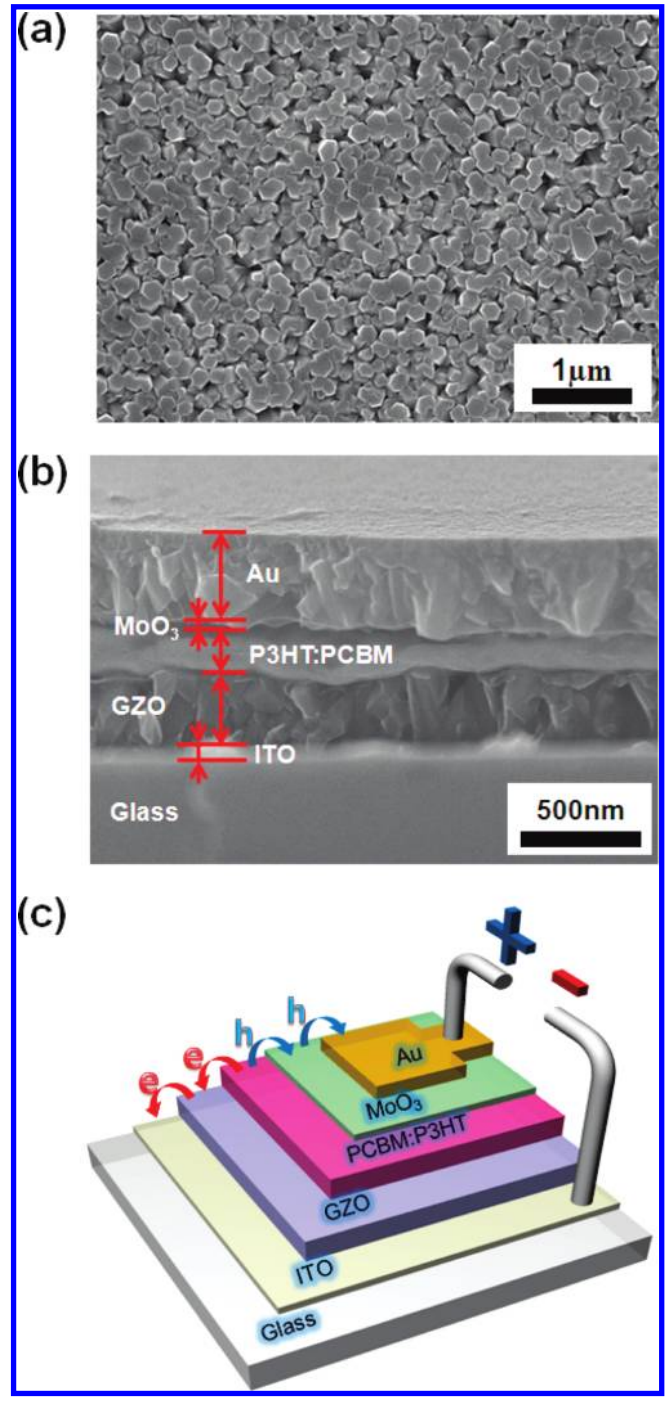

Figure 1. (a) Plan-view FE-SEM image of the GZO nanostructured thin film fabricated via an aqueous solution method. Cross-sectional FE-SEM image and schematic illustration of IOSCs with the GZO buffer layer as an electron-transport layer are shown in (b) and (c), respectively.

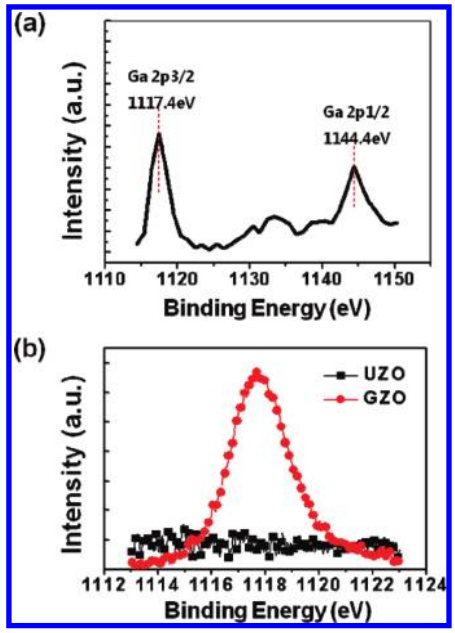

Figure 2. XPS results obtained from UZO and GZO thin films. (a) XPS spectrum for the Ga element in the GZO thin film. (b) Ga $2p_{3/2}$ peaks of the UZO and GZO thin films.

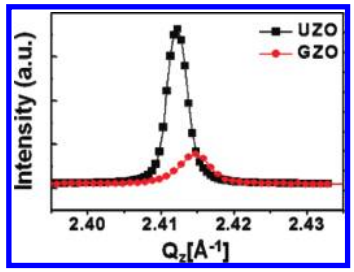

Figure 3. (002) diffraction peaks in powder diffraction profiles of UZO and GZO thin films using a synchrotron X-ray source.

the GZO buffer layer as compared with that of the UZO buffer layer, thus enhancing the J_{sc}.

The thickness of ZnO thin films in our devices is about 270 nm, which is much thicker than that in the previous work,[9] resulting in a decrease of the PCE due to deterioration of the transparency. We can further improve the PCEs of our IOSCs with either UZO or GZO by controlling thicknesses of a nanostructured ZnO layer. However, it is out of the scope of this work. We believe that the current PCEs (1.95% for GZO-based IOSCs and 0.92% for UZO-based IOSCs) are enough to evaluate our results for Ga-doping effects to the buffer layer in IOSCs.

In Hall-effect measurements based on the Van der Pauw configuration, the σ of the as-grown UZO and GZO thin films were measured as 3.4×10^{-3} $(\Omega cm)^{-1}$ and 7.2×10^{-3} $(\Omega cm)^{-1}$, respectively. At the initial stage of ZnO growth, nanorods are formed by the fastest growth along the *c* axis due to the high *c*-axis polar nature of ZnO. However, the preferred *c*-axis growth gradually saturates at a critical growth time. From this time, the growth of side facets of the nanorods proceeds, resulting in thin-film formation by the combination of individual rods.[19] Thus, it can be suggested that the relatively much lower conductivity values of the UZO and GZO thin films obtained by the Hall measurements in this work compared with those of ZnO thin films synthesized by other methods, such as sputtering, are due to hindrance of the electron transport in a lateral direction at the boundaries among the individual nanorods even though they are laterally connected to one another. However, the electron

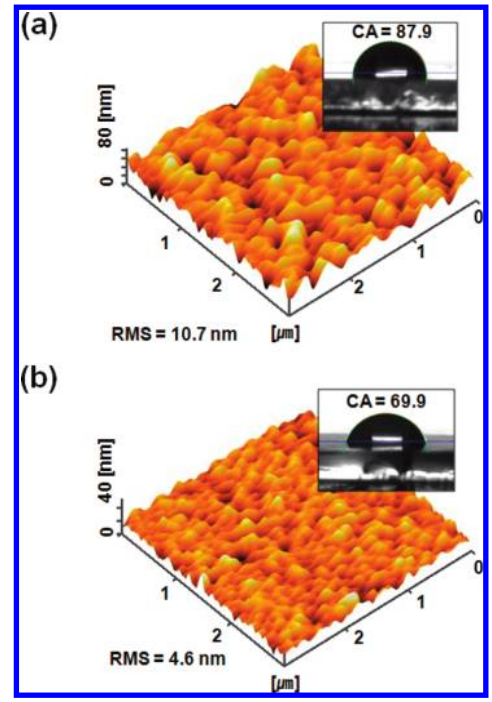

Figure 4. AFM images of (a) a UZO thin film and (b) a GZO thin film. The insets in (a) and (b) show CAs on UZO and GZO thin films, respectively.

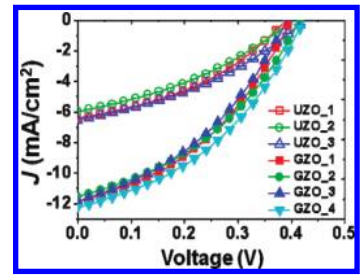

Figure 5. *J*−*V* characteristics for three UZO-based IOSCs and four GZO-based IOSCs under AM 1.5G irradiation.

transport along a vertical path into the thin film is more important for obtaining a large J_{sc} than that in a lateral path.

Because the series resistance (R_s, Ωcm^2) of an IOSC is strongly affected by the conductivity of the functional layers and their contact resistances, higher conductivity generally leads to a lower R_s.[20] The J_{sc} of an IOSC can be expressed as[21]

$$J_{sc} = (V_{dark} - V_{oc})/R_s \quad (1)$$

where V_{dark} is the intersection between the *x* axis and the *J*−*V* curve shifted by the J_{sc}. A low R_s can then generate the improved J_{sc} of an IOSC. Furthermore, a bimolecular recombination[22] can also be reduced through decrease of the R_s, resulting in enhancing the J_{sc}. It was found that the R_s of IOSCs with UZO and GZO thin films were 5.31 and 3.41 Ωcm^2, respectively, as determined by performing a mathematical simulation of the *J*−*V* curves in the dark shown in Figure 6 on the basis of eq 2

$$J(V) = J_0\{\exp[(V - JR_s)/nKT] - 1\} + (V - JR_s)/R_p - J_{sc} \quad (2)$$

where J_0 (mA/cm^2) is the reverse bias dark current and R_p (Ωcm^2) is the parallel resistance.[23] Thus, on the basis of the

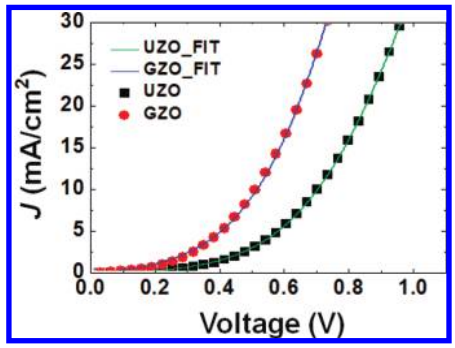

Figure 6. $J-V$ curves of two IOSCs (UZO_3 and GZO_4) investigated in Figure 5 under forward bias in the dark (symbols, experimental results; lines, simulated results).

enhancement factors of σ (7.2×10^{-3} from 3.4×10^{-3} $(\Omega\text{cm})^{-1}$), R_s (3.41 from 5.31 Ωcm^2), and J_{sc} (11.7 from 6.3 mA/cm^2) after Ga-doping, we suggest that the increase of the J_{sc} in a GZO-based IOSC is due to the higher conductivity of the GZO buffer layer, which decreases the R_s of devices, resulting in significant enhancement of the PCE.

As demonstrated in previous studies,[7,8] the J_{sc} is also strongly dependent on the morphology of the polymer. As shown in Figure 4, the CAs (69.9° for GZO and 87.9° for UZO) were affected by doping Ga into ZnO, which means that the surface energies of the films are different.[24−26] When a P3HT:PCBM polymer blend is spin-coated onto a buffer layer, the morphology of the polymer blend and the adhesion of interface between the polymer blend and the buffer layer are significantly changed by the surface energy of the buffer layer. In other words, the crystallinity of P3HT, the nanoscale phase separation of donor/acceptor, and improvement of the interface area for the electron conduction path are greatly affected by the wettability of the buffer layer.[7,20] Consequently, it can be proposed that the effective charge-carrier extraction and suitable phase segregation on a GZO-based IOSC yielded an improved J_{sc}, resulting in the dramatic enhancement of the PCE. Our results in this work suggest that such a doping approach can provide an excellent solution to enhance the PCE of IOSCs.

4. Conclusions

We have demonstrated a significant enhancement of the PCE in GZO-based IOSCs as compared with UZO-based IOSCs. XPS and synchrotron XRD results clearly showed that Ga atoms had been doped effectively into the ZnO lattices, resulting in the higher conductivity of GZO nanostructured thin films and thus mainly improving the J_{sc}. The rms roughness values and the grain sizes of the GZO thin films were less than those of the UZO thin films, and the water CA of GZO thin films exhibited a greater hydrophilicity than did that of the UZO thin films. Thus, it is suggested that the dramatic enhancement of the PCE of the GZO-based IOSCs is due to the higher electron conductivity and the favorable surface morphology of the grown GZO thin film.

Acknowledgment. This research was supported by the Basic Science Research Program through the National Research Foundation of Korea (NRF) funded by the Ministry of Education, Science and Technology (2010-0015035 and 2009-0077682) and also by the Gumi Digital Science Center Grant funded by the Korean government (MEST) (GDSC-002-081119-01). Synchrotron X-ray scattering experiments at Pohang Light Source were supported, in part, by the Ministry of Education, Science and Technology and POSTECH, Korea.

References and Notes

(1) Kim, J. Y.; Lee, K.; Coates, N. E.; Moses, D.; Nguyen, T. Q.; Dante, M.; Heeger, A. J. *Science* **2007**, *317*, 222–225.
(2) Li, G.; Shrotriya, V.; Huang, J.; Yao, Y.; Moriarty, T.; Emery, K.; Yang, Y. *Nat. Mater.* **2005**, *4*, 864–868.
(3) Padinger, F.; Rittberger, R. S.; Sariciftci, N. S. *Adv. Funct. Mater.* **2003**, *13*, 85–88.
(4) Chen, W. B.; Xiang, H. F.; Xu, Z. X.; Yan, B.-P.; Roy, V. A. L.; Che, C. M. *Appl. Phys. Lett.* **2007**, *91*, 191109.
(5) Chan, M. Y.; Lai, S. L.; Fung, M. K.; Lee, C. S.; Lee, S. T. *Appl. Phys. Lett.* **2007**, *90*, 023504.
(6) Halls, J. J. M.; Walsh, C. A.; Marseglia, E. A.; Friend, R. H.; Moratti, S. C.; Holmes, A. B. *Nature* **1995**, *376*, 498–500.
(7) Chen, L. M.; Hong, Z.; Li, G.; Yang, Y. *Adv. Mater.* **2009**, *21*, 1–16.
(8) Li, G.; Yao, Y.; Yang, H.; Shrotriya, V.; Yang, G.; Yang, Y. *Adv. Funct. Mater.* **2007**, *17*, 1636–1644.
(9) Yip, H. L.; Hau, S. K.; Baek, N. S.; Jen, A. K.-Y. *Appl. Phys. Lett.* **2008**, *92*, 193313.
(10) Park, W. J.; Shin, H. S.; Ahn, B. D.; Kim, G. H.; Lee, S. M.; Kim, K. H.; Kim, H. J. *Appl. Phys. Lett.* **2008**, *93*, 083508.
(11) Khranovskyy, V.; Grossner, U.; Nilsen, O.; Lazorenko, V.; Lashkarev, G. V.; Svensson, B. G.; Yakimova, R. *Thin Solid Films* **2006**, *515*, 472–476.
(12) Kyaw, A. K. K.; Sun, X.; Zhao, D. W.; Tan, S. T.; Divayana, Y.; Demir, H. V. *IEEE J. Sel. Top. Quantum Electron.* **2010**, in press. http://dx.doi.org/10.1109/JSTQE.2009.2039200.
(13) Choi, D.; Choi, M.-Y.; Shin, H.-J.; Yoon, S.-M.; Seo, J.-S.; Choi, J.-Y.; Lee, S. Y.; Kim, J. M.; Kim, S.-W. *J. Phys. Chem. C* **2010**, *114*, 1379–1384.
(14) Choi, M.-Y.; Choi, D.; Jin, M.-J.; Kim, I.; Kim, S.-H.; Choi, J.-Y.; Lee, S. Y.; Kim, J. M.; Kim, S.-W. *Adv. Mater.* **2009**, *21*, 2185–2189.
(15) Wang, H.; Baek, S.; Song, J.; Lee, J.; Lim, S. *Nanotechnology* **2008**, *19*, 075607.
(16) Rakhshani, A. E.; Bumajdad, A.; Kokaj, J.; Thomas, S. *Appl. Phys. A: Mater. Sci. Process.* **2009**, *97*, 759–764.
(17) Liang, S.; Bi, X. *J. Appl. Phys.* **2008**, *104*, 113533.
(18) Ahn, B. U.; Oh, S. H.; Hong, D. U.; Shin, D. H.; Moujoud, A.; Kim, H. J. *J. Cryst. Growth* **2008**, *310*, 3303–3307.
(19) Lee, S.-D.; Kim, Y.-S.; Yi, M.-S.; Choi, J.-Y.; Kim, S.-W. *J. Phys. Chem. C* **2009**, *113*, 8954–8958.
(20) Shaheen, S. E.; Ginley, D. S.; Jabbour, G. W. *MRS Bull.* **2005**, *30*, 10.
(21) Mette, A.; Pysch, D.; Emanuel, G.; Erath, D.; Preu, R.; Glunz, S. W. *Prog. Photovolt.: Res. Appl.* **2007**, *15*, 493–505.
(22) Pivrikas, A.; Juska, G.; Mozer, A. J.; Scharber, M.; Arlauskas, K.; Sariciftci, N. S.; Stubb, H.; Osterbacka, R. *Phys. Rev. Lett.* **2005**, *94*, 176806.
(23) Sze, S. M. *Physics of Semiconductor Devices*; Wiley-Interscience: New York, 1981; p 806.
(24) Kim, D.; Kim, J.; Hwang, W. *Surf. Sci.* **2006**, *600*, L301–L304.
(25) Shibuichi, S.; Yamamoto, T.; Onda, T.; Tsujii, K. *J. Colloid Interface Sci.* **1998**, *208*, 287–294.
(26) Rosario, R.; Gust, D.; Garcia, A. A.; Hayes, M.; Taraci, J. L.; Clement, T.; Dailey, J. W.; Picraux, S. T. *J. Phys. Chem. B* **2004**, *108*, 12640–12642.

JP1013658